Synthesis and characterization of magnetic and antibacterial nanoparticles as filler in acrylic cements for bone cancer and comorbidities therapy

Synthesis and characterization of magnetic and antibacterial nanoparticles as filler in acrylic cements for bone cancer and comorbidities therapy

Marta Miola[1*], Anuj Bellare[2], Roberto Gerbaldo[1], Francesco Laviano[1], Enrica Vernè[1]

[1] Institute of Materials Physics and Engineering, Department of Applied Science and Technology, Politecnico di Torino, C.so Duca degli Abruzzi 24, 10129 Torino, Italy

[2] Department of Orthopedic Surgery, Brigham & Women's Hospital, Harvard Medical School, 25 Shattuck Street, Boston, MA, 02115

* Corresponding author

Politecnico di Torino

Department of Applied Science and Technology, Politecnico di Torino, Torino (TO), Italy

Institute of Materials Engineering and Physics

Corso Duca degli Abruzzi, 24 - 10129 (TORINO) ITALY

Tel: +39 0110904717

Fax: +39 011 0904624

Abstract

In this work an innovative formulation of bone cement for the treatment of bone tumor and its associated complications has been designed by preparing a new class of Fe_3O_4-Ag nanostructures, using gallic acid as a reducing agent, and evaluating their introduction in different amounts and mixing method in polymethyl methacrylate (PMMA)-based composite cement. The morphology, the composition and antibacterial effect of Fe_3O_4-Ag nanostructures have been investigated together with the morphology, the composition, the mechanical

properties of the composite cements containing these nanoparticles as well as their antibacterial effect.

The obtained results revealed a good antimicrobial effect of Fe_3O_4-Ag nanostructures, a significant influence of their amount and of the used mixing method on the particles dispersion and agglomeration in the PMMA matrix and, as a result, on the mechanical properties. In particular, by using the mechanical mixing a better dispersion of nanoparticles was obtained, reducing the tendency to agglomerate. The increase of nanoparticles amount induced a slight decrease of the mechanical properties; however, the introduction of 10% w/w of Fe_3O_4-Ag allowed to improve the composites ability to reduce the bacteria adhesion.

Keywords

Magnetic nanoparticles; silver nanoparticles; bone cement; bone cancer; infection.

Introduction

Currently, surgery represents the most common approach to the treatment of primary and secondary bone tumours. This approach is very invasive, since it involves extensive local tissue removal or amputation, followed by reconstruction with prosthesis, acrylic bone cement, allograft or autograft and often causes serious disease [1-3]. The use of such invasive procedures in patients that are already immunocompromised implies intrinsic risks of bacterial contamination and development of extended infections [4].

Conventional therapies, such as chemotherapy and radiotherapy, are often used together with surgery [3], but they are often accompanied by severe side effects. Among the new therapies developed in recent years, such as immunotherapy and gene therapy [5, 6], hyperthermia has been documented as an effective approach to the treatment of solid tumors [7-9]. This therapy, as recognized by the European Society for Hyperthermic Oncology (ESHO) [10], uses

the application of high temperature (41-46 °C) in the vicinity of the tumors in the body, causing destruction to cancerous cells and tissues, while enhancing the efficacy of chemotherapeutic agents with very limited damage to healthy tissues.

Magnetically induced hyperthermia has been the object of investigation by many researchers [11]. This technique is targeted at the tumour site, and involves heat generation by means of magnetisable implants, which can be inserted into the void created by tumor removal and stimulated by exposure to an external alternating magnetic field to produce heat. This approach is safe for the surrounding healthy tissues and can be useful for a variety of solid tumours. With this purpose, various magnetic materials have been proposed in the literature, ranging from metallic particles (Fe, Co, Ni), oxides (Fe_2O_3, Fe_3O_4), ferrites ($LiFe_5O_8$, $MgFe_2O_4$), magnetic fluids, up to magnetic bone cements and glass-ceramics [12-24]. Only a few of these materials have been also adapted to be able to prevent the primary associated complications of bone tumor surgery, such as the development of infections [25, 26]. For example, in the recent work published by Miola et al. [26] a silver-containing ferrimagnetic glass–ceramic (Ag-SC45) has been developed and characterized, showing the ability to generate heat when exposed to an alternating magnetic field and possessing a documented antibacterial effect. In previous studies [27] Miola et al. have been also developed innovative bioactive superparamagnetic nanoparticles for multifunctional composite bone cements, which displayed bioactive behavior for the first time in literature. The aim of the present work is to introduce a new class of superparamagnetic nanoparticles with magnetic and antibacterial properties, as filler for acrylic bone cement that can be used to destroy cancer cells by hyperthermia and to reduce the prevalence of infections.

1. Experimental

According to literature [28, 29] and previous research works of the authors [30 - 32] the steps for synthesis and decoration of magnetite nanoparticles (MNPs) can be summarized as follows:

• Synthesis of MNPs using co-precipitation method and their dispersion in water using citric acid (CA)

• Coating of CA capped MNPs with a silica shell, by sol-gel process, to obtain magnetite-silica NPs (MSNPs)

• Modification of silica shell by *in situ* silver reduction to obtain MSNPs decorated with Ag NPs (MSAgNPs)

1.1 Synthesis of citric acid (CA) capped MNPs

The co-precipitation method was adapted from literature [28]. In detail, two solutions of ferrous and ferric iron salts ($FeCl_2$ and $FeCl_3$) were prepared separately: 37.5 ml of 0.1 M $FeCl_2$ and 50 ml 0.1 M $FeCl_3$ were mixed under mechanical stirring at 300 rpm. The pH of this solution was between 1.5-2. Ammonia was added drop by drop until a pH=10 was attained. This step promoted the precipitation of magnetite nanoparticles and the color of the solution turned from orange-yellow to black. Since the synthesis was carried out in air, also maghemite precipitation can occur. In order to prevent agglomeration, the solution was sonicated for 20 minutes (Sonica®, ultrasonic cleaner, SOLTEC®) and then washed 2 times with bi-distilled water.

The MNPs were dispersed in CA to prevent agglomeration. A solution of 0.05 M CA was prepared and added to the nanoparticles magnetically separated from water. The concentration of the CA solution was selected based on the literature [28][30-32]. After the pH of the MNPs + CA suspension reached a value of approximately 2.5-3 the pH was raised to about 5.2 with ammonia in order to increase the rate of adsorption [28]. In fact, it is reported that at this pH CA presents two deprotonated carboxylic groups, which can interact with the -

OH groups exposed on MNPs surface. Subsequently, the solution was kept in an orbital shaker (KS 4000i control, IKA®) at 80 °C and 150 rpm for 90 minutes**.** Finally, the solution was washed with bi-distilled water to remove the unreacted citric acid and the pH was set to about 10.1 (by ammonia addition) in order to maximize the nanoparticles dispersion in water. The setting of pH at 10.1 was necessary for the de-protonation of the third -COOH group of CA, to impart a negative surface charge to the particles and promote their dispersion in water for electrostatic repulsion [28]. The washing steps were performed using an ultrafiltration device (Solvent Resistant Stirred Cells - Merck Millipore).

1.2 Synthesis of silica-coated magnetite NPs (MSNPs) decorated with silver nanoparticles (MSAgNPs)

The synthesis of MSAgNPs followed a preliminary coating of MNPs with a silica shell. According to literature [29], the Stöber process was used in order to create a silica layer around the nanoparticles, using tetraethyl orthosilicate (TEOS) as silica precursor. The amount of TEOS was chosen in order to obtain a shell thickness of about 1 nm, as reported in literature [33]. Firstly, the MNPs + CA suspension was centrifuged at 4000 rpm for 5 minutes. In a second step, water was removed by ultrafiltration, then CA capped MNPs were re-suspended in a mixture of water and ethanol (ratio 4:1) [34] and the silica shell precursors solution was added drop by drop (0.33 ml of TEOS, 3 ml of water and 3 ml of ethanol for 40 ml of MNPs suspension). After the addition of this solution to the MNPs suspension, the pH was increased up to 11 with dropwise ammonia and the suspension was maintained for 3 h in orbital shaker at 37 °C. Subsequently, the suspension was filtered to remove ethanol by ultrafiltration, and washed twice with bi-distilled water. Finally, the silica-coated MNPs (MSNPs) were suspended in water. With the aim to impart antibacterial activity, silver nanoparticles were synthetized *in situ* on the MSNPs surface using silver nitrate ($AgNO_3$) as precursor and gallic acid (GA) as a reducing

agent, producing MSNPs decorated with silver nanoparticles (MSAgNPs). The amount of silver nitrate with respect to the desired amount of silver nanoparticles was selected on the basis of literature for similar synthesis[34]. For 20 ml of MSNPs suspension, two $AgNO_3$ amounts were investigated (8 and 17 mg).

Firstly, $AgNO_3$ was added to the suspension of MSNPs. The suspension was mechanically stirred at 300 rpm for 10 minutes, then ammonia was added dropwise to set the pH = 11, causing the deprotonation of hydroxyl ligands on the silica surface and the electrophilic attack of Ag^+ at the deprotonated silica shell [34]. Secondly GA (molar ratio $AgNO_3$/GA = 1.7) [35] was added with mechanical stirring at 300 rpm for 10 minutes to reduce $Ag(NH_3)^{2+}$ to Ag NPs on the surface of MS NPs and pH was set once again around 11. At the end, the solution was washed twice with bi-distilled water and the pH decreased to about 10. The proposed mechanism for MSAgNPs synthesis is reported in figure 1.

1.3 Preparation of nanocomposite bone cement

The first step in the procedure to synthesize composite bone cements required the dispersion of NPs, dried at 60 °C, in methyl methacrylate (MMA) in an ultrasound bath for 20 minutes. Subsequently the solution of NPs and MMA was mixed with pre-polymerized polymethyl methacrylate (PMMA) powders according to the procedure described in [27].

The bone cement used in this study was Surgical Simplex© P (Stryker Orthopaedics Inc, Mahwah, NJ), one of the most commonly used bone cements in clinic applications. It contains $BaSO_4$ as radiopaque agent.

The preparation methods and the type of mixing have been tailored in order to assure a good dispersion and an accurate quantity of the various NPs in the PMMA matrix, to enable good compressive strength and antibacterial properties.

The composite cements were developed by mixing the following components:

- Surgical Simplex© P powder component (named simply PMMA from now on): 15 wt% PMMA-styrene copolymers, 75 wt% PMMA, 10 wt% barium sulphate as radio-opaque phase and 1.5 wt% benzoyl peroxide initiator;
- Surgical Simplex© P liquid component (named simply MMA from now on): 97.5 wt% MMA, 89 ppm hydroquinone stabilizer and 2.6 wt% NN Dimethyl P Toluidine activator;
- Magnetic NPs

The plain commercial Surgical Simplex© P cement was used as a control material.

1.3.1 Hand mixing and mechanical mixing

Cement preparation was performed in a sterile cartridge (PRISM II vacuum mixing cartridge, DePuy). The Prism II system allowed mixing and collection under vacuum in a closed system. Using this kit two different types of specimens were prepared for each synthesis, the first type with hand mixing and the second one with mechanical mixing.

Hand mixing is the method normally used in operating room and the mix is prepared with a suitable inert device with a manually stirring action (with plastic stirrer) until the powder is completely saturated with the liquid. While, for the mechanical mixing evacuated the Prism II mixer was used but the mix was prepared with mechanical stirring. This second method is expected to provide a better dispersion of NPs and materials mixing, but its use in a real surgical application needs to be investigated, because current protocols dictate that motors and electrical devices should be avoided in the operating room unless necessary. In order to determine the appropriate range of blending speeds, preliminary compressive tests were performed on cements obtained using different mixing speeds. Pure Surgical Simplex© was used for this test and the speed of 1500 rpm was chosen on the basis of obtained results [27].

1.3.1.1 Plain bone cement

The cements were prepared according to the manufacturers' instructions at room temperature. The PMMA powder/MMA liquid weight ratio was maintained at 2:1.

The two components (powder and liquid) were mixed in the cartridge of PRISM II system under vacuum for about 1 minute with the hand mixing and always under vacuum but for about 30 seconds with mechanical mixing; then the cartridge was transferred to a cement gun and the cement was injected into steel molds to produce cylindrical (6 ∅ x12 mm) samples for compressive test according to ISO 5833-2002 [36].

1.3.1.2 Magnetic nanocomposite bone cement

The concentration of magnetite suspension was estimated gravimetrically as about 4.5 ± 0.5 mg of MNPs for 1 ml of suspension. Taking into account this concentration, the nanocomposite bone cements were produced with two different amounts of MNPs, 5 wt% and 10 wt%, respectively.

The suspension of MNPs was dried in an oven at 60 °C to minimize particles agglomeration. The dried powders were gently ground in a mortar to break up the agglomerates. Figure 2a shows the dried MNPs attracted by a magnet. After drying and grinding, the MNPs powders were mixed with the liquid monomer and sonicated for 20 minutes to remove residual agglomerates. Each cement was prepared by mixing the PMMA powder with the liquid (MMA+MNPs) in PRISM II under vacuum cartridge for 1 minute (hand mixing) and thereafter for 30 seconds (mechanical mixing).

The injection in the molds and the polymerization step were carried out with the same modalities used for plain commercial bone cement, as described previously.

1.3.1.3 Magnetic and antibacterial nanocomposite bone cement

The concentration of magnetic and antibacterial suspension was again measured gravimetrically, estimated to be about 3.5 ± 0.5 mg/ml of MSAgNPs. The preparation of the nanocomposites containing MSAgNPs was performed following the same previously described procedure for the magnetic nanocomposite bone cement.

The synthesis II was selected to synthesize the antibacterial and magnetic bone cements on the basis of obtained results from the antibacterial efficacy of MSAgNPs.

Table 1 summarizes the synthesized composite bone cements, evidencing the used mixing method and amount of NPs.

Sample name	**Mixing method**	**NPs (wt%)**
Simplex© P	Hand	-
Simplex© P+MNPs	Hand	Magnetite (5%)
Simplex© P+MNPs	Hand	Magnetite (10%)
Simplex© P+MSAgNPs	Hand	Magnetite-Silica-Ag (10%)
Simplex© P	Mechanical	-
Simplex© P+MNPs	Mechanical	Magnetite (5%)
Simplex© P+MNPs	Mechanical	Magnetite (10%)
Simplex© P+MSAgNPs	Mechanical	Magnetite-Silica-Ag (10%)

Table 1: Sample name, mixing method and amount of NPs introduced.

1.4 Morphological and compositional characterization

All the nanoparticles were characterized by means of field emission scanning electron microscopy equipped with energy dispersive spectroscopy (FESEM-EDS, SUPRA™ 40, Zeiss) and scanning transmission electron microscopy (STEM, Merlin Gemini Zeiss) to investigate their morphology, shape and dimensional range, as well as to estimate their composition, the

presence of the silica layer and the grafting with Ag nanoparticles. The nanocomposite bone cements were observed by the same methodologies, to evaluate the dispersion of the nanoparticles embedded in the polymeric matrix.

1.5 Antibacterial properties

The antibacterial properties of the Ag-doped nanoparticles were evaluated by the inhibition halo test (Kirby Bauer test) in accordance with National Committee for Clinical Laboratory Standards (NCCLS standard [37]). The test was performed against *Staphylococcus aureus* ATCC 29213 bacterial strain, one of the strains most commonly involved in post-surgical infections [38]. Three circular (10 mm in diameter) disks of filter paper were impregnated with a drop of MSAgNPs suspension and were placed on a Mueller Hinton agar plate uniformly covered with bacteria, as recommended by NCCLS standard and reported in [39]. The plate with the samples was incubated overnight at 35 °C. At the end of the incubation the possible formation of a halo (inhibition zone) around the sample, in which the bacteria have not proliferated was observed and measured. When no inhibition halo was observed, the plate was inverted to determine whether the bacteria had proliferated below the sample or not: the absence of bacterial proliferation under samples is however an index of good antibacterial effect.

The evaluation of the antibacterial properties of the nanocomposite bone cements was performed following the same steps conducted for the MSAgNPs suspension. In this case, the composite cement samples were placed on a Mueller Hinton agar plate uniformly covered with bacteria and the plate was incubated overnight at 35 °C. At the end of the incubation the possible formation of a halo around the sample was observed, also by inverting the plate to verify the possible bacterial proliferation below the sample. Moreover, samples were subjected to heat fixation procedure to fix cells eventually adhered on cement surface [40]. Heat fixation was performed by the rapid passage of samples for three times over the flame of

a Bunsen burner; subsequently, samples were prepared for SEM observation by metallization with a thon Cr layer.

All reagents were purchased from Becton, Dickinson and Company.

1.6 Mechanical properties

The mechanical properties of the cements were evaluated by measuring the compressive strength of the cement samples in accordance with the standard ISO 5833:2002 [36].

To prepare the cylindrical specimens needed for the compression test, the cement paste was poured into a stainless steel mold containing 5 holes (diameter= 6 mm, height = 12 mm) and clamped with stainless steel sheets. After cement hardening, the cylindrical samples were removed from the mold. After 24 ± 2 h, the diameter of the cement cylinder was precisely measured with plane-parallel ends, and it was placed upright in the test device. The superior and inferior faces were machined with a laser cut edge and polished with abrasive paper in order to create two plain and parallel surfaces. The specimens were placed in the test machine (ADMET-type mechanical testing, Nanotechnology Laboratory at the Orthopedic Surgery Department of the Brigham and Women's Hospital in Boston, USA) without any type of pad between the cylinder and the plate of the test machine, that was set up to produce a curve of displacement against load, using a constant cross-head speed of 25 mm/min at room Temperature (approximately 21 °C) in air and force were measured by a 10000 lbf (4444.4 N) capacity load cell. The compression loading continued until there was a decline in load. The maximum strength was used to calculate the compressive strength. Compressive strength of acrylic bone cement, to be in compliance with ISO 5833:2002, must be $\geq$ 70 MPa [36, 41].

The compressive strength, after drawn the line at 2% offset load, was calculated for each specimen as the ultimate load divided by the original cross-sectional area. The average compressive strength of five cylinders for each different type of material was calculated.

1.7 Magnetic properties

The magnetic properties of composite cements containing 10 wt% of MNPs, MSNPs and MSAgNPs, mechanically mixed, were investigated with a DC magnetometer/ AC susceptometer (Lakeshore 7225) equipped with a Cryogen-Freemagnet at room temperature in quasi static condition.

Magnetic hysteresis cycle measurements were performed using a magnetic field up to 800 kA/m, in order to estimate the main magnetic parameters of the materials and possible differences between the two samples.

2. Results and discussion

2.1 MNPs

Figure 2b illustrates the FESEM images of the obtained MNPs, which showed a spherical shape and a dimensional range of 5-20 nm. The EDS analysis (Figure 2d) showed the presence of Fe and O peaks, elements characteristic of magnetite (the presence of Cu and C are due to the grid used for the analysis).

The MNPs were also characterized by STEM. In line with the FESEM results, STEM analysis showed magnetite nanoparticles with a pseudo-spherical morphology and a dimensional range between 5-20 nm (Figure 2c).

2.2 MSNPs

STEM analysis of MSNPs, reported in figure 2e, revealed nanoparticles with a size around 5-20 nm (Figure 3a), and EDS analysis showed the presence of the Si peak (Figure 2f). The presence and the thickness of the silica shell was also confirmed by previous studies [30, 32].

The silica shell acted as a supporting matrix for the Ag NPs to anchor, in order to solve the problem of aggregation of the Ag NPs. Furthermore, the silica shell could also protect the Fe_3O_4 core from being oxidized and dissolved in water solution, which enhanced the stability of the MSAgNPs. Hence, an antibacterial material having a characteristic magnetic response and enhanced stability could be obtained.

2.3 MSAgNPs

The *in situ* synthesis of silver NPs using gallic acid was verified by means of STEM-EDS analysis. Gallic acid ($C_6H_2(OH)_3COOH$) is one of the common aromatic compounds having both carboxylic and phenolic groups. It is a natural plant phenol found in green tea, red wine and grapes with antioxidant and bactericide properties. GA was used as a reducing and stabilizing agent [42]. The oxidation reaction of phenol groups in gallic acid was responsible for the reduction of silver ions, and the produced quinoid compound with a ketoenol-system could be adsorbed on the surface of magnetic nanoparticles accounting for their stabilization.

2.3.1 Synthesis I

Figure 3a,b shows the STEM analysis of MSAgNPs nanoparticles obtained using 0.017 g of $AgNO_3$ (synthesis I). MSAgNPs always showed a pseudo-spherical shape and a dimensional range slightly higher.

EDS analysis (Figure 3c) revealed the peaks associated with Fe, Si and Ag.

This analysis showed the presence of some aggregates of Ag particles of about 100 nm (visible in dark field mode-DF, figure 3a). However, several well distributed Ag nanoparticles with smaller size (about 10-30 nm) were also evident (backscattering mode, figure 3b); the obtained Ag nanoparticles created a nanodumbell with magnetic nanoparticles.

EDS analysis was also performed to verify the composition of the samples; figure 3c shows the peaks of the elements distinctive of the MSAgNPs. The analysis in an area apparently not

containing Ag revealed the presence of the silver peak; this may indicate the presence of very small Ag nanoparticles unidentifiable by STEM analysis.

2.3.2 Synthesis II

Figure 3d,e shows the MSAgNPs nanoparticles prepared in the second synthesis. In this case, small spherical nanoparticles were also observed with a dimensional range between 5-20 nm. Moreover, STEM analysis always showed the presence of big Ag clusters (approximately 100 nm in size) visible in gray in STEM dark field mode (DF, Figure 3d) together with Ag NPs with smaller size (20-30 nm, Figure 3e) well distributed within the sample.

EDS analysis (Figure 3f) confirmed the presence of Ag, Fe, Si and O peaks, characteristic of MSNPs. However, contrary to synthesis I, in synthesis II EDS analysis did not show the presence of Ag when an area apparently not containing Ag was analyzed. This likely means that in the second synthesis Ag particles with sizes less than 20-30 nm were not formed.

2.4 Nanocomposite bone cements morphological and compositional characterization

2.4.1 Hand mixed bone cement

FESEM analysis in backscattering mode (QBSD) of pure Simple P (Figure 4) reveal the presence of PMMA sphere, in dark gray, and barium sulphate powders in white, together with some $BaSO_4$ agglomerates.

2.4.1.1 Synthesis of 5% w/w MNPs/PMMA hand mixed composite bone cement

The synthesis of 5% w/w MNPs/PMMA composite bone cement was performed according to the procedure explained in the experimental section. The performed FESEM-EDS analysis (reported in [27]) revealed the presence of zones where MNPs were well dispersed and

distributed in the PMMA matrix and other areas containing some MNPs agglomerates of tens of μm, together with the presence of some $BaSO_4$ agglomerates, as in reference samples.

2.4.1.2 Synthesis of 5% w/w MSAg NPs/PMMA hand mixed composite bone cement

The same analysis was conducted for MSAgNPs/PMMA composite bone cement samples. The obtained results are reported in figure 5 and are very similar to results obtained for MNPs.

FESEM-EDS analysis of composite bone cement revealed some areas with $BaSO_4$ agglomerates (Figure 7a,b), the presence of some MSAgNPs agglomerates (Figure 5a,c), smaller than $BaSO_4$ agglomerates, and areas without agglomerates (Figure 5a,d). At higher magnification, it was possible to observe the presence of MSAgNPs well dispersed in the PMMA matrix (Figure 5e,f).

This result indicated that the chosen process to prepare the nanocomposite bone cement still needs optimization. As reported in [27], the presence of agglomerates is believed to be due to the hand mixing process that does not allow for good dispersion.

Therefore, the nanocomposite optimization and characterization were focused on the introduction of mechanical mixing of NPs.

2.4.2 Synthesis of 5% w/w MNPs/PMMA composite bone cement mechanically mixed

On the basis of FESEM-EDS results, it was evident that this method provided a better dispersion of NPs and materials mixing, reducing the voids and improving the mechanical properties (Figure 6).

A reduction of the agglomerates and their size was obtained (Figure 6a,b), while the EDS analysis in areas without NPs agglomerates showed the presence of the characteristic elements of the nanoparticles (Figure 6b,c)

2.4.2.1 Synthesis of 5% w/w MSAg NPs/PMMA composite bone cement mechanically mixed

Again, in this case, the mechanical mixing reduced the number of agglomerates and their size, as it can be observed in FESEM-EDS analysis of Figure 7.

2.4.2.2 Synthesis of 10% w/w MNPs/PMMA composite bone cement mechanically mixed

In order to enhance the magnetic and antibacterial properties of the composites, 10 wt% of NPs was added to the polymeric matrix. In this case, since the mechanical mixing results were better than hand mixing, the composite samples were prepared using mechanical mixing.

Figure 8 shows the morphological and compositional analysis of 10% w/w MNPs/PMMA composite bone cement mechanically mixed. The image and spectra reveal a good dispersion of MNPs in the PMMA matrix and, also in this case, a reduction of the dimensions of MNPs aggregates.

2.4.2.3 Synthesis of 10% w/w MSAg NPs/PMMA composite bone cement mechanically mixed

The FESEM analysis in QBSD mode (Figure 9) of composites containing 10 wt% of MSAgNPs showed few and small NPs aggregates (Figure 9b). EDS analysis in areas apparently devoid of agglomerates revealed the presence of the characteristic elements of the nanoparticles (Figure 9a).

2.5 Mechanical Compression test

PMMA-based bone cements are brittle in nature. PMMA bone cements show low tensile strength but quite high compression strength [43, 44]. Bone cement is subjected to very high stresses during human activity (about 3 times of body weight when walking); in particular, when it is used to fix protheses, it is subjected to compression and shear [43, 45]. Moreover, it has been verified that the introduction of a second ceramic phase can decrease the

compressive strength of the cement [44], due to weak interfacial strength produced between these two phases. For these reasons, and since the measurement of the compressive strength is required by the current standard for set and cured cement (ISO 5833:2002 [36]) [46], this study focuses on compressive strength.

If NPs are inserted as filler in a small amount (like 5% w/w MNPs-PMMA sample) and distributed homogeneously in the cement dough (mechanical mixing) the mechanical properties can be preserved. If the proportion of the nanoparticles increases, this could lead to non-homogeneous distribution and, therefore, aggregation of particles may occur. This may cause the presence of large defects in the structure and poor adhesion to the matrix leading to a decrease in the compressive strength.

As shown in Figure 10, in general the addition of hard nanoparticles in a PMMA-based bone cement decreased the mechanical properties.

All the compressive strength values of different samples decreased with respect to the value obtained for pure cement; in particular the values are subthreshold, defined by the ISO standard, when hand mixing is adopted. Using the mechanical mixing the compressive strength increases since a better NPs dispersion and voids reduction were achieved, as also demonstrated by other studies [47]. Finally, an increase in the amount of NPs slightly decreased the compressive strength.

2.6 Magnetic characterization

The hysteresis cycles for composite cements containing MNPs, MSNPs and MSAgNPs up to 800 kA/m are reported in Figure 11. The obtained curves show a typical behavior of a superparamagnetic material: no evidence of remnant magnetization and coercivity was observed. The saturation magnetization (Ms) of MNPs reached about 30 Am^2/Kg , of MS sample 21 Am^2/Kg, while Ms of MSAg sample was around 15 Am^2/Kg. As reported in [30],

considering the weight of silica coatings and the Ag nanoparticles, it can be assumed that the magnetic properties of both composites are similar.

2.7 Antibacterial test on MSAg NPs

The inhibition halo test was conducted for each MSAgNPs batch (synthesis I and II). Figure 12 shows the formation of an inhibition halo of about 2-3 mm for both samples.

The halo consists of two zones, the first area of about 1 mm for sample with NPs synthesis I and 1.5 mm for sample with NPs synthesis II, within which the proliferation of bacteria is completely inhibited and a second area within the first bacterial colonies begin to proliferate. Even if the performed test is semi-quantitative and the dimension of the halo obtained with synthesis I is slightly larger than that obtained with synthesis II, the obtained results suggest that the bacteria proliferated less (first zone, where the bacterial growth was completely inhibited.) around the sample obtained with synthesis II. Then, as previously mentioned, the synthesis II was selected to synthesize the antibacterial and magnetic bone cements, since the obtained particles present suitable dimension and optimal antibacterial test.

2.8 Antibacterial test of nanocomposite bone cement

The halo inhibition test was conducted for each antibacterial nanocomposite bone cement, which differ from for MSAgNPs amount and/or mixing method. Unfortunately, any composite samples revealed the presence of an inhibition zone; for this reason, to verify the possible bacterial adhesion on samples surface FESEM measurements were carried out on samples exposed to the burner flame for few seconds, 3 times, to fix bacterial cells on samples surfaces.

Figure 13 shows the images of the composites containing 5 wt% of MSAgNPs, hand mixed, after inhibition halo test. As it can be observed, the analysis revealed the presence of bacteria

adhered on the sample surface, but on the areas around MSAg NPs agglomerates (evidenced with a dashed line) a reduced bacterial adhesion was observed (Figure 13b).

This means that the nanoparticles embedded in the PMMA matrix have a local antibacterial effect.

FESEM analysis performed on composites containing 5 wt% of MSAgNPs mechanically mixed showed the presence of bacteria adhered in some areas of the sample surface (Figure 13d); however, several areas with limited bacterial adhesion were observed (Figure 13c).

The more uniform dispersion of NPs obtained using the mechanical mixing improved the antibacterial effect.

Figure 13e-f reports the FESEM images of composites containing 10 wt% of MSAgNPs; it is possible to observe areas with a limited number of adhered bacteria (Figure 13f) and areas almost free of adhered bacteria (Figure 13e). Then, the morphological analysis revealed a lower presence of bacteria adhered to the surface of this stock of cements in comparison with those synthesized with 5% of nanoparticles. The evaluation of adhered cells by means of colonies count unit (CFU) test should be performed in order to better and quantitatively measure statistically significant differences.

3. Conclusions

In conclusion, the Fe_3O_4-Ag nanocomposite structures designed and characterized in this work have been successfully optimized as additional phase of an innovative and promising formulation of bone cement for the treatment of bone tumor and its associated complications. The results concerning the morphology, the composition and the mechanical properties of the composite cements revealed a significant influence of the NPs amount and of the used mixing method on the particles dispersion and agglomeration in the PMMA matrix and, as a result, on the mechanical properties. In particular, the tendency to agglomeration can be reduced by

using mechanical mixing procedures, which are associated to a better dispersion of NPs. The increase of NPs amount induced a slight decrease of the mechanical properties. In spite of this issue, the characterization of the composite cements for their antibacterial effect revealed that the introduction of 10% w/w of MSAg NPs improves the ability to reduce the bacteria adhesion. On the base of these results, it can be assessed that the introduction of magnetic and antibacterial nanoparticles into PMMA-based matrix can be a promising approach to obtain multifunctional stimuli-responsive composite bone cements for the treatment of bone tumors and associated complications. It must be noted that the amount and dispersion of the magnetic and antibacterial nanoparticles must be optimized in order to provide the necessary thermal and antibacterial effects without compromising mechanical properties that are necessary for clinical use. Future works will be dedicated to the improvement of antibacterial properties and will verify the cement heating ability in hyperthermia treatment.

Acknowledgements

The authors would like to acknowledge Dr. Fucale Giacomo (Chemical, Clinical and Microbiological Analyses Dept., CTO, Turin, Italy.) for its assistance during antibacterial test.

References

[1] A.K. Freeman, V.P. Sumathi, L. Jeys, Primary malignant tumours of the bone, Surgery (Oxford) 26 (2015) 27-34. https://www.surgeryjournal.co.uk/article/S0263-9319(17)30226-0/fulltext. doi:10.1016/j.mpsur.2008.12.009

[2] A.K. Freeman, V.P. Sumathi, L. Jeys, Metastatic tumours of bone, Orthopaedics I: General Principles, Surgery (Oxford) 36 (2018) 35–40. https://www.surgeryjournal.co.uk/article/S0263-9319(17)30227-2/pdf. DOI:https://doi.org/10.1016/j.mpsur.2017.10.002

[3] G. Selvaggi, G.V. Scagliotti, Management of bone metastases in cancer: A review, Critical Reviews in Oncology/Hematology 56 (2005) 365–378. https://www.sciencedirect.com/science/article/abs/pii/S1040842805000661

[4] D. Campoccia, L. Montanaro, C.R. Arciola The significance of infection related to orthopedic devices and issues of antibiotic resistance, Biomaterials 27 (2006) 2331–39. https://www.sciencedirect.com/science/article/pii/S0142961205010938. doi:10.1016/j.biomaterials.2005.11.044

[5] K. Mori, F. Redini, F. Gouin, B. Cherrier, D. Heymann Osteosarcoma: current status of immunotherapy and future trends (Review), Oncology Reports, Spandidos Publications, 15 (3) (2006) 693-700. https://pubmed.ncbi.nlm.nih.gov/16465432/

[6] F.A. Scappaticci, N. Marina, New molecular targets and biological therapies in sarcomas, Cancer Treat. Rev, 27 (2001) 317-326. https://pubmed.ncbi.nlm.nih.gov/11908925/

[7] P. Wust, B. Hildebrandt, G. Sreenivasa, B. Rau, J. Gellermann, H. Riess, et al. Hyperthermia in combined treatment of cancer. Lancet Oncol. 3 (2002) 487, 2002. https://pubmed.ncbi.nlm.nih.gov/12147435/

[8] B. Hildebrandt , P. Wust , O. Ahlers , A. Dieing , G. Sreenivasa , T. Kerner , R. Felix , H. Riess, The cellular and molecular basis of hyperthermia, Crit Rev Oncol Hematol. 43(1) (2002) 33-56. https://pubmed.ncbi.nlm.nih.gov/12098606/

[9] A. Bettaie, P.K. Wrzal, D.A. Averill-Bates, Hyperthermia: Cancer Treatment and Beyond. Medicine, Oncology, "Cancer Treatment - Conventional and Innovative Approaches", book edited by Letícia Rangel , ISBN 978-953-51-1098-9, Published: May 9, 2013 under CC BY 3.0 license. © The Author(s). Chapter 12 DOI: 10.5772/55795

[10] http://www.esho.info/professionals/hyperthermia/description/index.html, visited 20/04/2020.

[11] D. Chang, M. Lim, J.A.C.M. Goos, R. Qiao, Y.Y. Ng, F.M. Mansfeld, M. Jackson, T.P. Davis5,7 and Maria Kavallaris1,3* Biologically Targeted Magnetic Hyperthermia: Potential and Limitations. Front. Pharmacol., 02 August 2018 | https://doi.org/10.3389/fphar.2018.00831

[12] A. Matsumine, K. Kusuzaki, T. Matsubara, K. Shintani, H. Satonaka, T. Wakabayashi, S. Miyazaki, K. Morita, K. Takegami, A. Uchida, Novel hyperthermia for metastatic bone tumors with magnetic materials by generating an alternating electromagnetic field, Clin. Exp. Metastasis. 24 (2007) 191–200. https://link.springer.com/article/10.1007/s10585-007-9068-8?shared-article-renderer

[13] M.M. Cruz, L.P. Ferreira, A.F. Alves, S.G.Mendo, P. Ferreira, M. Godinho, M.D. Carvalho, Chapter 19 - Nanoparticles for magnetic hyperthermia. Nanostructures for Cancer Therapy Micro and Nano Technologies (2017) 485-511

[14] O. Bretcanu, E. Verné, M. Cöisson, P. Tiberto, P. Allia Magnetic properties of the ferrimagnetic glass-ceramics for hyperthermia, J Magn Magn Mater 305 (2006) 529-533. https://www.sciencedirect.com/science/article/abs/pii/S0304885306003969

[15] O. Bretcanu, E. Vernè, M. Cöisson, P. Tiberto, P. Allia Temperature effect on the magnetic properties of the coprecipitation derived ferrimagnetic glass-ceramics, J Magn Magn Mater 300 (2006) 412- 417. https://www.sciencedirect.com/science/article/abs/pii/S0304885305005809.

[16] O. Bretcanu, S. Spriano, C. Vitale-Brovarone, E. Vernè, Synthesis and characterization of coprecipitation-derived ferrimagnetic glass-ceramic, J Mater Sci 41 (2006) 1029-1037. https://link.springer.com/article/10.1007/s10853-005-2636-x

[17] O. Bretcanu, S. Spriano, E. Vernè, M. Coisson, P. Tiberto, P. Allia The influence of crystallized Fe3O4 on the magnetic properties of coprecipitation-derived ferrimagnetic glass-ceramic, Acta Biomaterialia 1 (2005) 421-429. https://pubmed.ncbi.nlm.nih.gov/16701823/

[18] A. Cochis, M. Miola, O. Bretcanu, L. Rimondini, E. Vernè, Magnetic Bioactive Glass Ceramics for Bone Healing and Hyperthermic Treatment of Solid Tumors. Ashutosh Tiwari et al. (eds.) Advanced Magnetic and Optical Materials, (81–112) © 2017 Scrivener Publishing LLC

[19] M. Miola, Y. Pakzad, S. Banijamali, Saeid Kargozar, C. Vitale-Brovarone, A. Yazdanpanah, O. Bretcanu, A. Ramedani, E. Vernè, M. Mozafari, Glass-ceramics for cancer treatment: So close, or yet so far? Acta Biomaterialia 83 (2019) 55-70. https://www.sciencedirect.com/science/article/abs/pii/S1742706118306676

[20] O. Bretcanu, M. Miola, C.L. Bianchi, I. Marangi, R. Carbone, I. Corazzari, M. Cannas, E. Verné, In vitro biocompatibility of a ferrimagnetic glass-ceramic for hyperthermia application. Mater Sci Eng C Mater Biol Appl. 2017 Apr 1;73:778-787. doi: 10.1016/j.msec.2016.12.105. Epub 2016 Dec 23. https://pubmed.ncbi.nlm.nih.gov/28183672/

[21] M.V. Velasco 2 , M.T. Souza, C. Murilo, A.J. Aparecido de Oliveira, E.D. Zanotto. Bioactive magnetic glass-ceramics for cancer treatment. Biomedical Glasses 5 (2019) 148-177. https://www.degruyter.com/view/journals/bglass/5/1/article-p148.xml?language=en

[22] S. Mohapatra, R. Mishra, P. Roy, et al. Systematic investigation and in vitro biocompatibility studies on implantable magnetic nanocomposites for hyperthermia treatment of osteoarthritic knee joints. J Mater Sci 52 (2017) 9262–9268. https://doi.org/10.1007/s10853-017-1136-0

[23] M. Bruno, M. Miola, O. Bretcanu, C. Vitale-Brovarone, R. Gerbaldo, F. Laviano, E. Verné, Composite bone cements loaded with a bioactive and ferrimagnetic glass-ceramic. Part I: Morphological, mechanical and calorimetric characterization, J Biomater Appl. 29(2) (2014) 254-267. https://pubmed.ncbi.nlm.nih.gov/24505077/

[24] E. Verné, M. Bruno, M. Miola, G. Maina, C. Bianco, A. Cochis, L. Rimondini, Composite bone cements loaded with a bioactive and ferrimagnetic glass-ceramic:Leaching, bioactivity

and cytocompatibility, Mat. Sc. Eng, C. 53 (2015) 95-103. https://pubmed.ncbi.nlm.nih.gov/26042695/

[25] L.G. Shapeero, B. Poffyn, P.J.L. De Visschere, G. Sys, D. Uyttendaele, D. Vanel, R. Forsyth, K.L. Verstraete, Complications of bone tumors after multimodal therapy. Eur J Radiol 77 (2011) 51–67. https://www.sciencedirect.com/science/article/abs/pii/S0720048X1000389X

[26] M. Miola, R. Gerbaldo, F. Laviano, M.Bruno, E. Verne`, Multifunctional ferrimagnetic glass–ceramic for the treatment of bone tumor and associated complications. J Mater Sci 52(13) (2017) 9192–9201. https://link.springer.com/article/10.1007/s10853-017-1078-6 DOI 10.1007/s10853-017-1078-6

[27] M. Miola, A. Bellare, F. Laviano, R. Gerbaldo, E. Verné, Bioactive superparamagnetic nanoparticles for multifunctional composite bone cements. Ceramics International. 45(12) 2019 14533-14545. https://www.sciencedirect.com/science/article/pii/S0272884219309952

[28] S. Campelj , D. Makovec, M. Derofenik, Preparation and properties of water-based magnetic fluid, J.Phys.Condens. Matter 20 2008 101-104. https://pubmed.ncbi.nlm.nih.gov/21694231/

[29] W. Stöber, A. Fink, Controlled growth of monodisperse silica spheres in the micron size range, J. Colloid Interface Sci. 26 (1968) 62–69. https://www.sciencedirect.com/science/article/abs/pii/0021979768902725

[30] E. Borroni, M. Miola, S. Ferraris, et al. Acta Biomaterialia, Tumor targeting by lentiviral vectors combined with magnetic nanoparticles in mice. 2017;59:303-316. doi:10.1016/j.actbio.2017.07.007.

[31] M. Miola, S. Ferraris , F. Pirani, C. Multari, E. Bertone, K. Žužek Rožman, N. Kostevšek, E. Verné, Reductant-free synthesis of magnetoplasmonic iron oxide-gold nanoparticles, Ceramics International 43 (2017) 15258–15265. https://www.sciencedirect.com/science/article/pii/S0272884217317625

[32] G. Muzio, M. Miola, S. Ferraris, M. Maggiora, E. Bertone, M.P. Puccinelli, M. Ricci, E. Borroni, R.A. Canutoa, E. Verné, A. Follenzi, Innovative superparamagnetic iron-oxide nanoparticles coated with silica and conjugated with linoleic acid: Effect on tumor cell growth and viability Materials Science and Engineering C 76 (2017) 439–447. https://pubmed.ncbi.nlm.nih.gov/28482548/

[33] E. Cheraghipour, S. Javadpour, R. Ali Mehdizadeh, Citrate capped superparamagnetic iron oxide nanoparticles used for hyperthermia therapy J Biomed Sci Eng 5(12) (2012) 715-719. https://www.scirp.org/journal/paperinformation.aspx?paperid=25767

[34] X. Zhang, H. Niu, J. Yan, Y. Cai, Immobilizing silver nanoparticles onto the surface of magnetic silica composite to prepare magnetic disinfectant with enhanced stability and antibacterial activity, Colloids and Surfaces A: Physicochem. Eng. Aspects 375 (2011) 186–192. https://www.sciencedirect.com/science/article/pii/S0927775710007302

[35] G.A. Martínez-Castañón, N. Niño-Martínez, F. Martínez-Gutierrez, et al. Synthesis and antibacterial activity of silver nanoparticles with different sizes, J Nanopart Res (2008) 10: 1343. https://doi.org/10.1007/s11051-008-9428-6

[36] International standard ISO 5833 “Implants for surgery — Acrylic resin cements” Second edition 2002-05-01.

[37] M2-A9, Performance Standards for Antimicrobial Disk Susceptibility Tests, Approved Standard, 9th Edn, NCCLS, Villanova, PA, USA 2003.

[38] D. Campoccia, L. Montanaro, P. Speziale, C.R. Arciola, Antibiotic-loaded biomaterials and the risks for the spread of antibiotic resistance following their prophylactic and therapeutic clinical use, Biomaterials 31 (2010) 6363–6377. https://pubmed.ncbi.nlm.nih.gov/20542556/

[39] M. Miola, E. Vernè, Bioactive and Antibacterial Glass Powders Doped with Copper by Ion-Exchange in Aqueous Solutions. Materials 2016, 9, 405. https://www.ncbi.nlm.nih.gov/pmc/articles/PMC5456756/

[40] A. Rozar, Practical Methods for Environmental Microbiology and Biotechnology, by P.G. Engelkirk, and J. Duben-Engelkirk EdD MT(ASCP) Oct 8, 2007.

[41] K.D. Kuhn, Bone Cement Up-to-Date Comparison of Physical and Chemical Properties of Commercial Materials, SPRINGER, 2000

[42] S. Ferraris, M. Miola, A. Cochis, B. Azzimonti, L. Rimondini, E. Prenesti, E. Vernè, In situ reduction of antibacterial silver ions to metallic silver nanoparticles on bioactive glasses functionalized with polyphenols. Applied Surface Science 396 (2017) 461–470. https://www.sciencedirect.com/science/article/abs/pii/S0169433216323157

[43] S. M. Zebarjad, S. A. Sajjadi, T. Ebrahimi Sdrabadi, A. Yaghmaei, B. Naderi. A Study on Mechanical Properties of PMMA/Hydroxyapatite Nanocomposite. Engineering 3(8) (2011) 795-801. doi: 10.4236/eng.2011.38096. https://www.scirp.org/pdf/ENG20110800011_69374755.pdf

[44] K. Serbetci, F. Korkusuz and N. Hasirci, Thermal and Mechanical Properties of Hydroxyapatite Impregnated Acrylic Bone Cements, Poly-mer Testing 23 (2004) 145-155. https://www.sciencedirect.com/science/article/pii/S0142941803000734 doi:10.1016/S0142-9418(03)00073-4

[45] H. Khellafi, M.M. Bouziane, A. Djebli, A. Mankour, M. Bendouba, B. Bachir Bouiadjra, E. Ould Chikh. Investigation of Mechanical Behaviour of the Bone Cement (PMMA) Under Combined Shear and Compression Loading. Journal of Biomimetics, Biomaterials and Biomedical Engineering, 41 (2019) 37-48. https://www.scientific.net/JBBBE.41.37

[46] C. Lee. Properties of Bone Cement: The Mechanical Properties of PMMA Bone Cement, In: The Well-Cemented Total Hip Arthroplasty. Springer, Berlin, Heidelberg, 2005.

[47] L. Lidgren, B. Bodelindl, J. Myller, Bone cement improved by vacuum mixing and chilling Acta Orthop. Scand. 57 (1987) 27-32. https://pubmed.ncbi.nlm.nih.gov/3577737/

Figures captions

Figure 1: Synthesis steps of MSAgNPs.

Figure 2: dried MNPs attracted by a magnet (a), FESEM (b), STEM (c) and EDS (d) analysis of MNPs, STEM (e) and EDS (f) analysis of MSNPs

Figure 3: STEM (a, b) and EDS (c) analysis of MSAgNPs – synthesis I, STEM (d, e) and EDS (f) analysis of MSAgNPs – synthesis II.

Figure 4: FESEM analysis of Simplex© P bone cement acquired in QBSD mode.

Figure 5: FESEM-EDS analysis of MSAgNPs/PMMA composites.

Figure 6: FESEM-EDS analysis of MNPs/PMMA composite bone cement mechanically mixed.

Figure 7: FESEM-EDS analysis of MSAgNPs/PMMA composite bone cement mechanically mixed.

Figure 8: FESEM-EDS analysis of 10% w/w MNPs/PMMA composite bone cement mechanically mixed.

Figure 9: FESEM-EDS analysis of 10% w/w MSAgNPs/PMMA composite bone cement mechanically mixed.

Figure 10: compressive strength of reference cement and composites.

Figure 11: magnetic measurements of M, MS and MSAg NPs.

Figure 12: inhibition halo test of MSAgNPs batch synthesis I and II.

Figure 13: SEM images of composites containing 5 wt% of MSAgNPs hand mixed (a, b), 5 wt% of MSAgNPs mechanically mixed (c, d), 10 wt% of MSAgNPs (e, f).

Figures

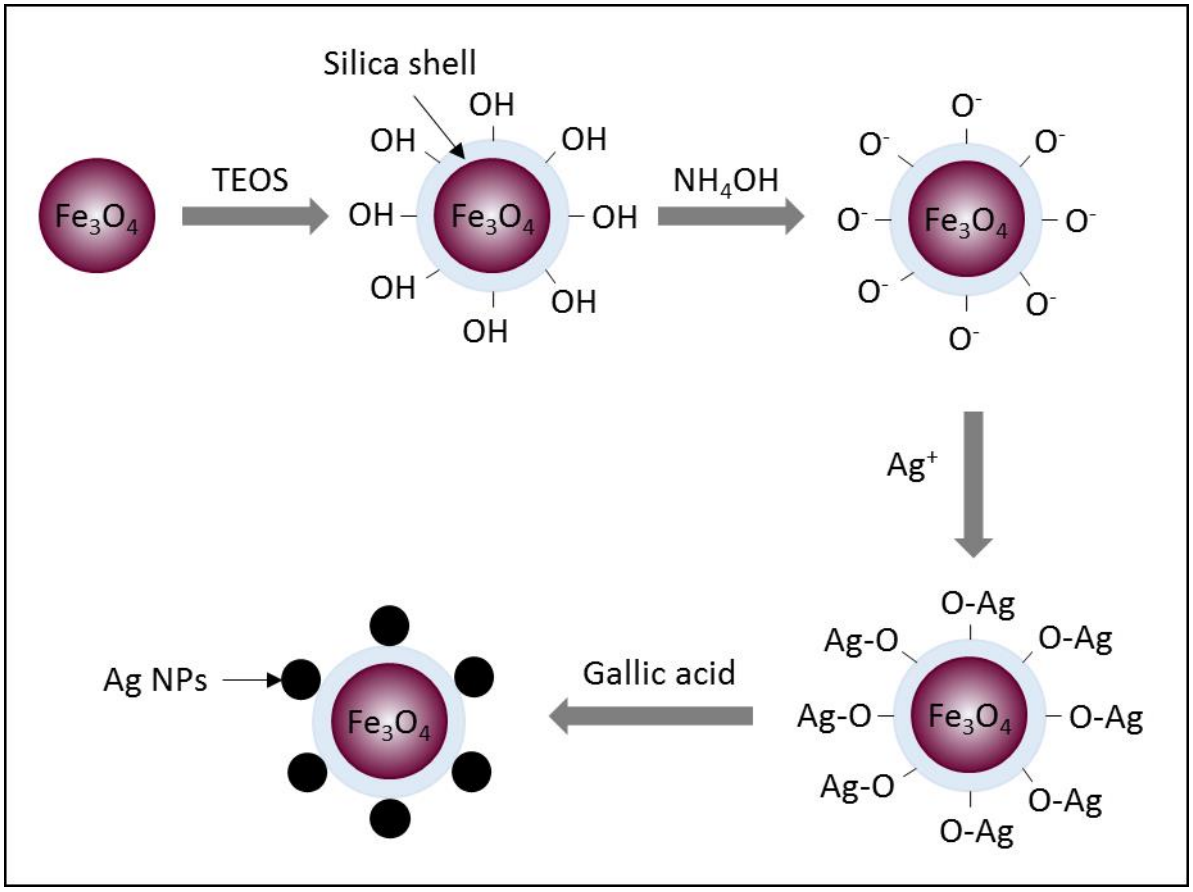

Figure 1

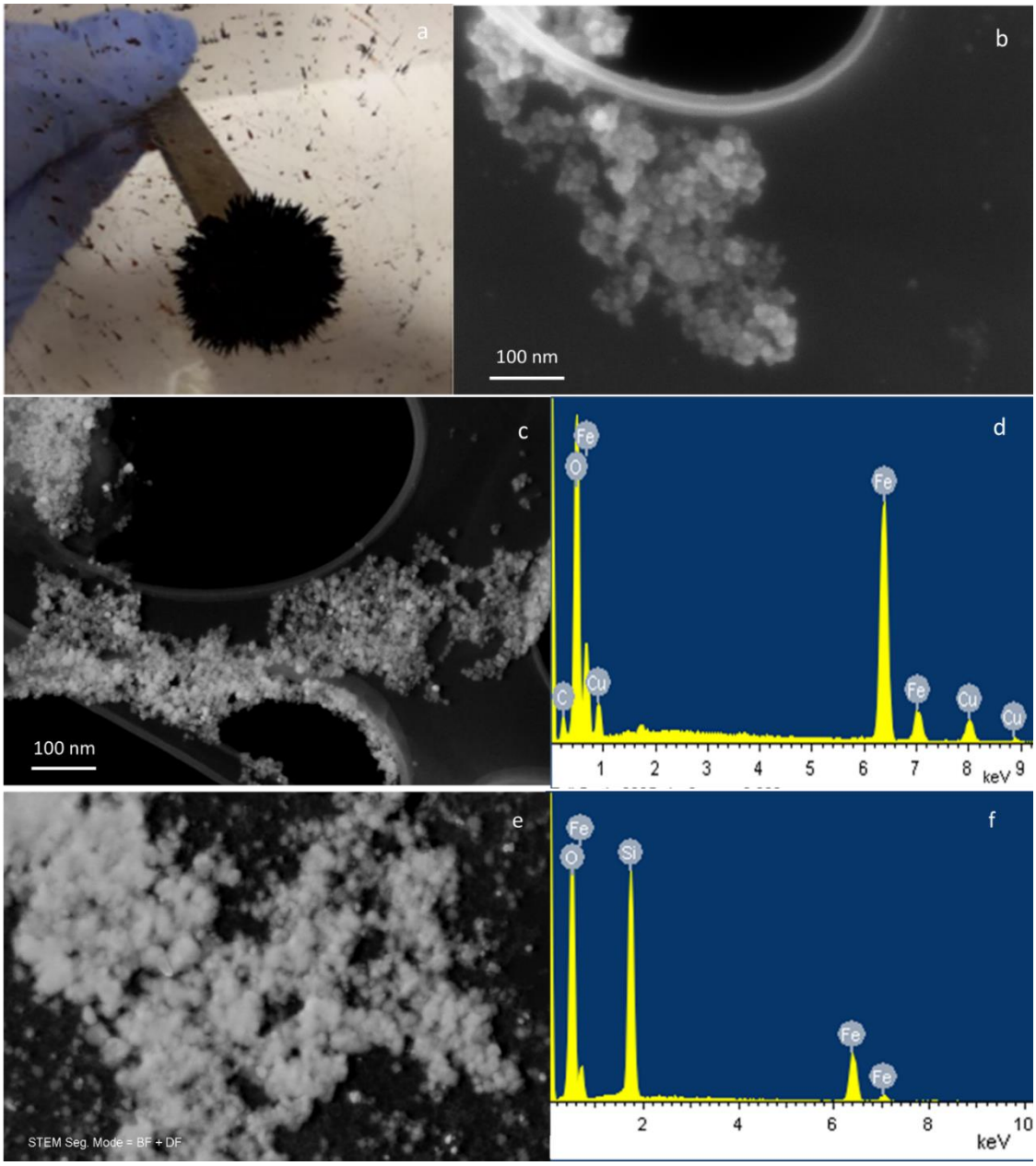
a
b
100 nm
c
100 nm
d
Fe
O
Fe
C
Cu
Fe
Cu
Cu
1
2
3
4
5
6
7
8
keV
9
e
STEM Seg. Mode = BF + DF
f
Fe
O
Si
Fe
Fe
2
4
6
8
10
keV

Figure 2

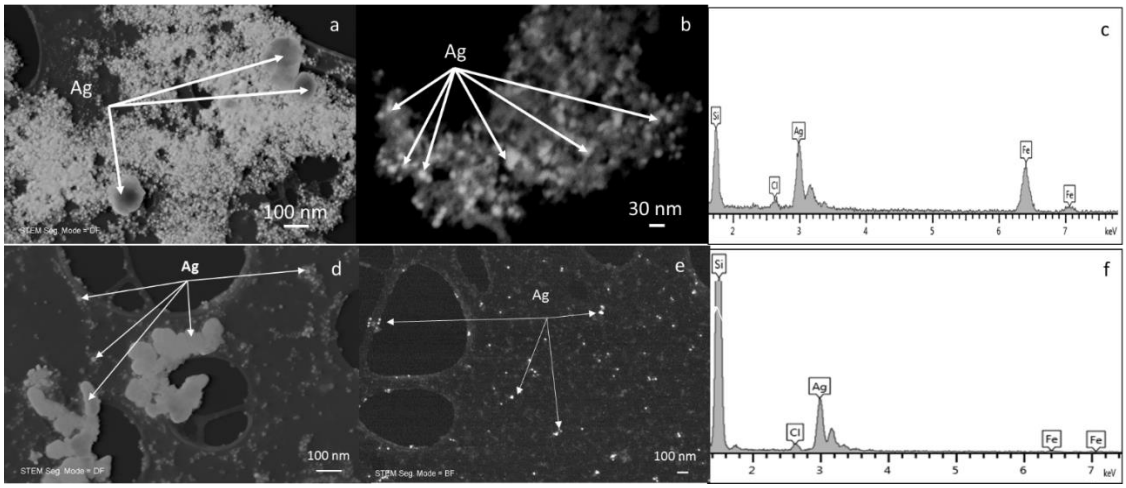

Figure 3

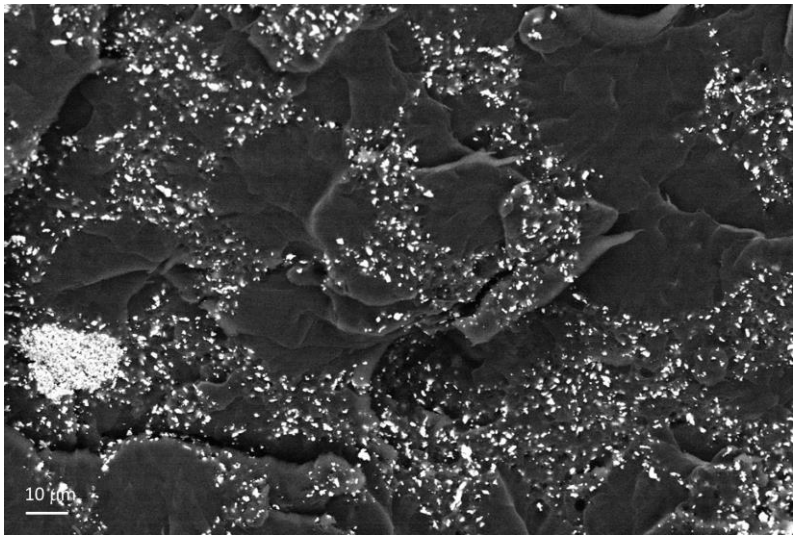

Figure 4

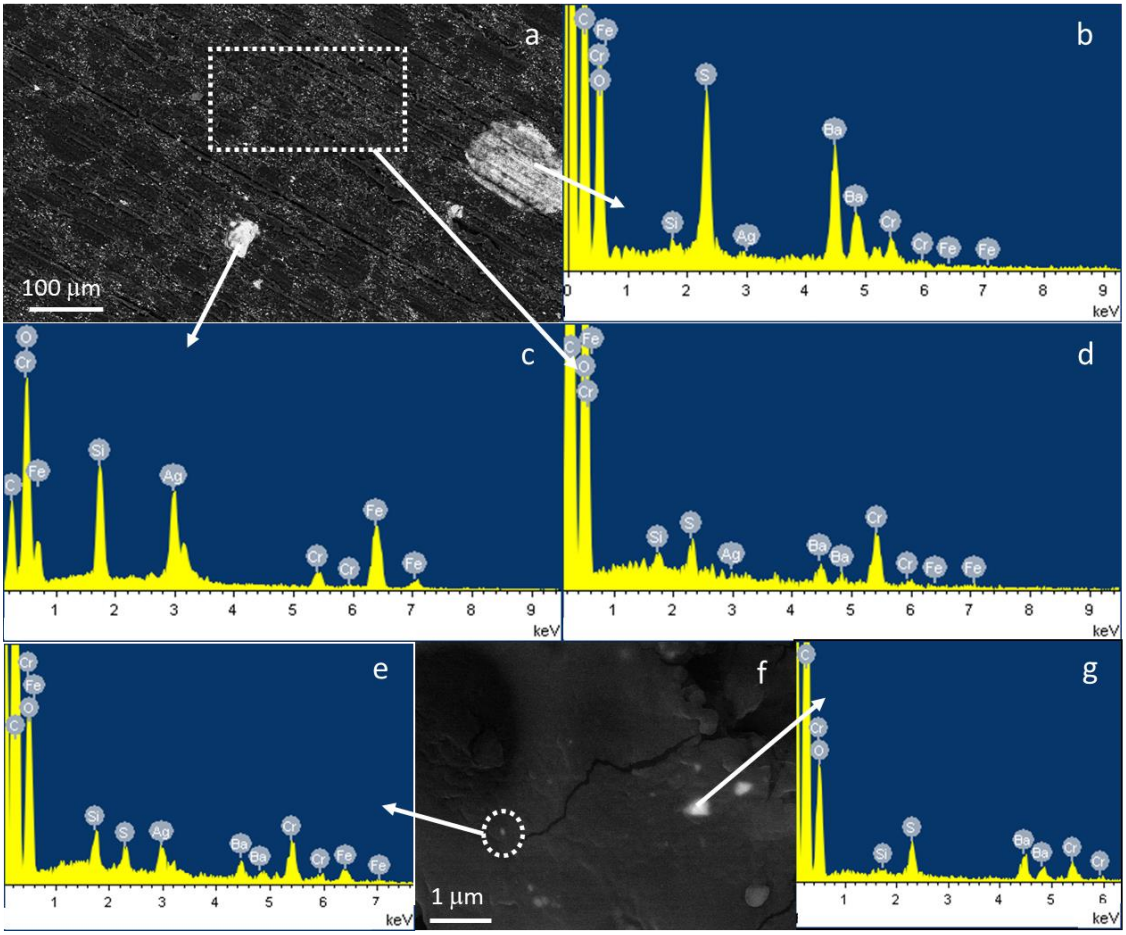

Figure 5

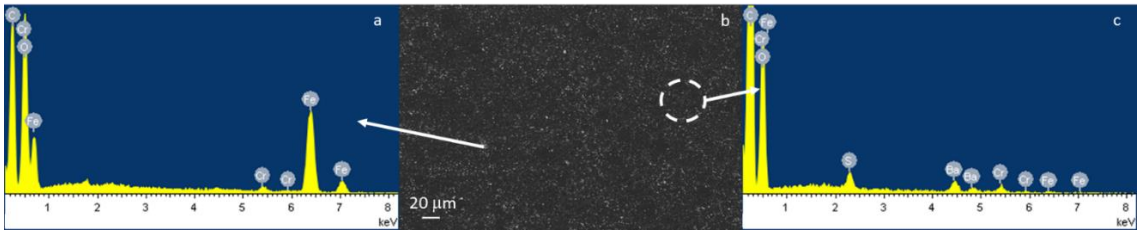

Figure 6

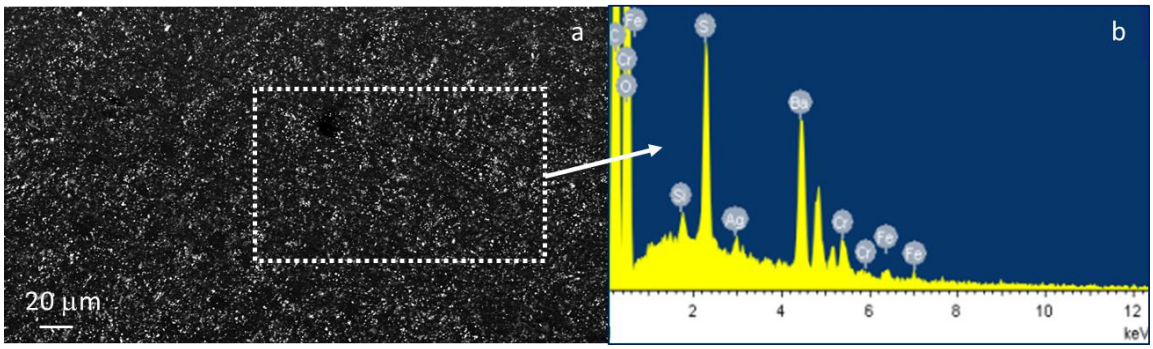

Figure 7

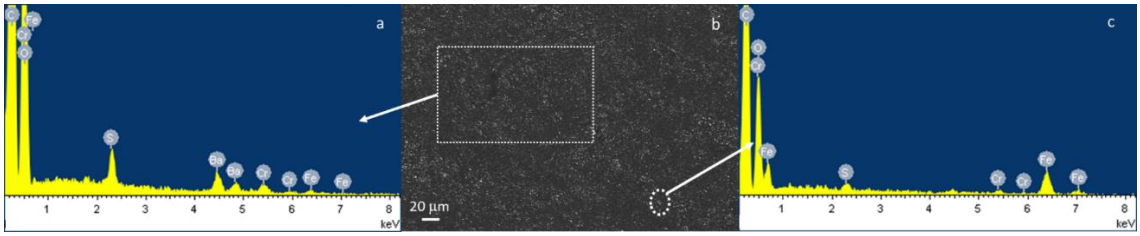

Figure 8

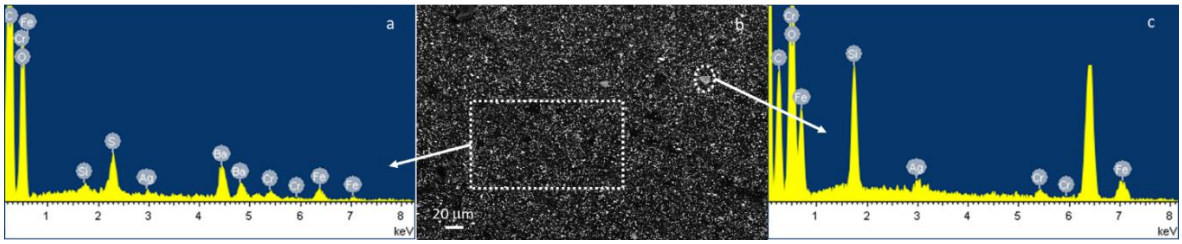

Figure 9

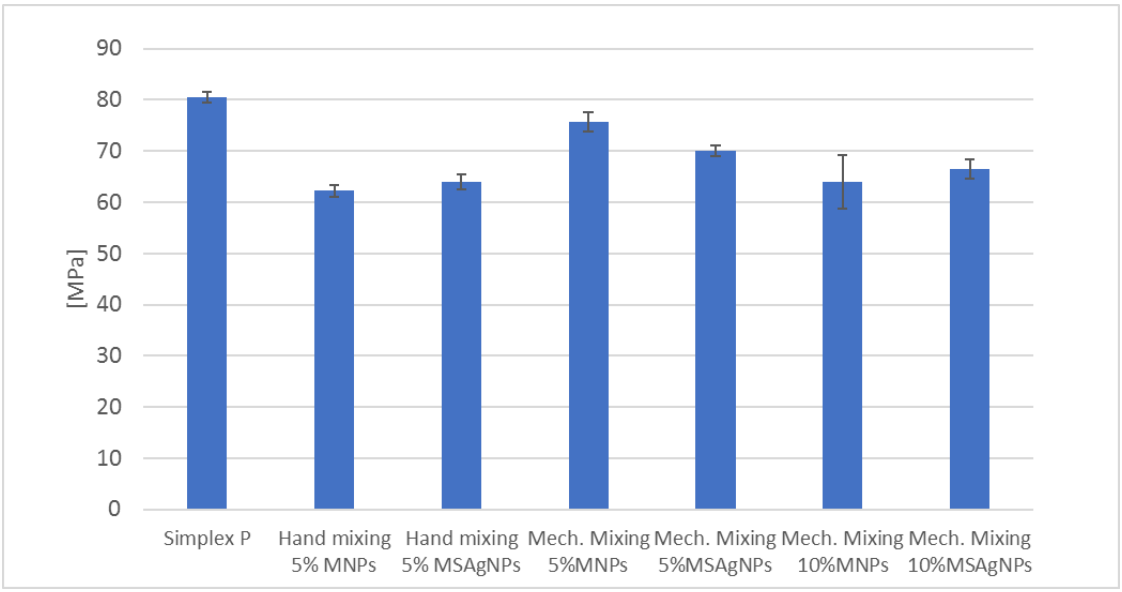

Figure 10

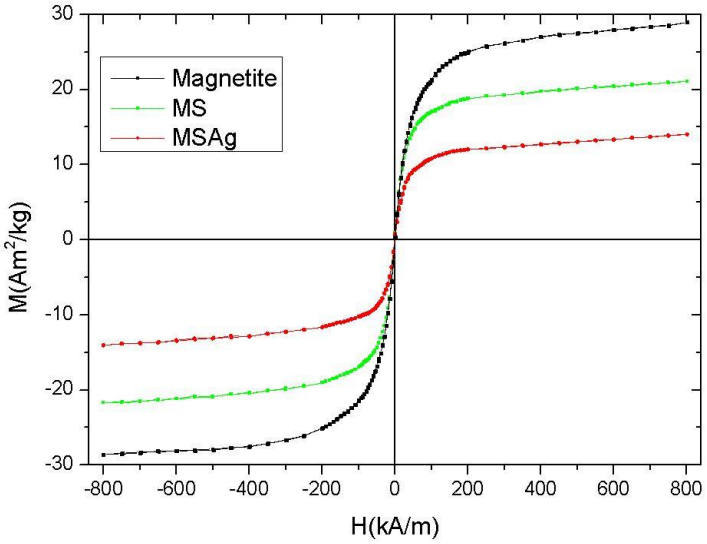

Figure 11

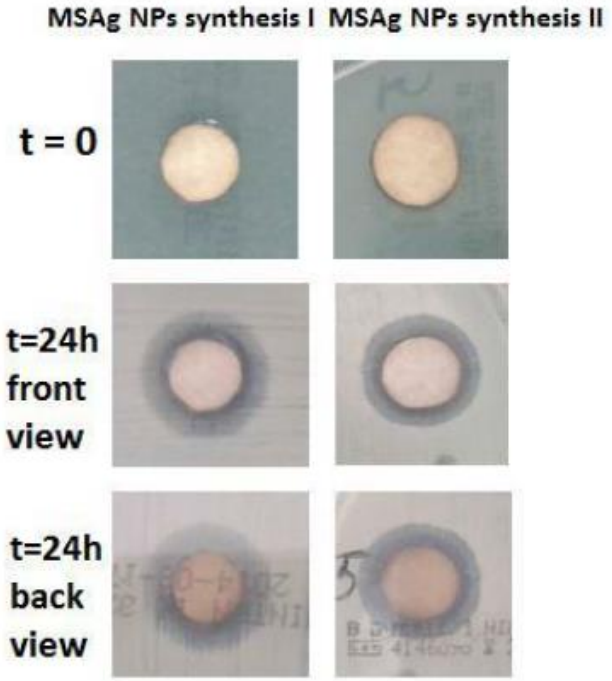

Figure 12

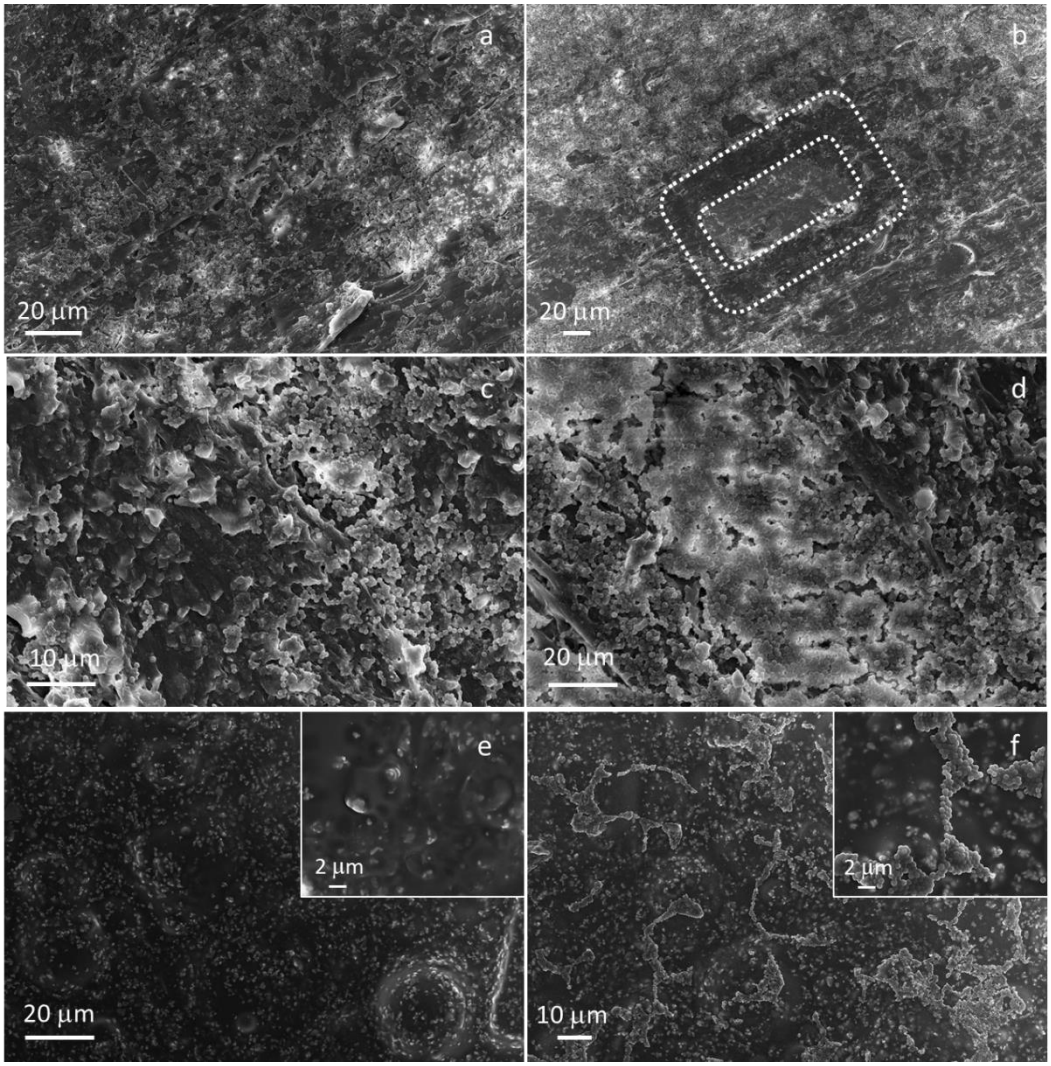

Figure 13